Kinetics of high-density plasmas generated in Si by 1.06- and 0.53-μm picosecond laser pulses

Henry M. van Driel
Department of Physics and Erindale College, University of Toronto, Toronto, Canada M5S 1A7
(Received 11 June 1986; revised manuscript received 2 October 1986)

The dynamics of high-density ($10^{19} < N < 10^{21}$ cm^{-3}), high-temperature ($300 < T_e < 3000$ K) plasmas, generated in silicon by single 1.06- and 0.53-μm picosecond laser pulses, is simulated with a self-consistent model based on the Boltzmann transport equation. Balance equations, which include possible plasma degeneracy effects, are used to obtain the spatial and temporal evolution of the lattice temperature as well as the carrier density and temperature. We compare predictions of the model, which employs parameters extracted from near-equilibrium experiments, with data from recent experiments which measured the melt threshold or time-dependent infrared reflectivity. The model is able to account quantitatively for the weak dependence of the melt threshold on pulse width at 0.53 μm as well as the strong dependence at 1.06 μm. In the former case, direct absorption and lattice parameters dominate energy evolution, but at 1.06 μm two-photon absorption and plasma dynamics dominate. The infrared reflectivity measurements are found to be consistent with a simple Drude model of the dielectric constant and the calculated plasma kinetics when one accounts for nonzero probe pulse widths and plasma spatial inhomogeneity. When this is done there is no need to introduce ultrashort momentum relaxation times or plasmon assisted recombination as speculated on in the recent literature. Finally, contrary to earlier suppositions, it is found that the carrier temperature can exceed the lattice temperature by more than 10^3 K during pulses as long as 100 psec even for subpicosecond carrier-phonon relaxation times. It is also found that the carrier temperature exhibits two peaks as a function of time, one due to direct laser heating of the carriers and the other due to Auger heating.

I. INTRODUCTION

Recently, there has been considerable interest in the kinetics of high-density, ambipolar plasmas generated in silicon by ultrashort laser pulses.[1-8] From a fundamental viewpoint there has been a desire to achieve a knowledge of the properties of highly nonequilibrium plasmas while an applied viewpoint has addressed the possible role of plasmas in aiding or initiating melting. Typically, the silicon is excited and monitored on subnanosecond time scales using optical techniques such as reflectivity[5] or transmission.[4,6] Because of the complex dynamics which determine the spatial and temporal evolution of the plasmas on these time scales, it is often difficult to isolate one process and extract information about it. In many cases the interpretation of results is also hampered or misled by an incomplete or inconsistent model of the plasma dynamics or even of the optical response. In this paper we consider a self-consistent model based on linear transport theory and, as an example, use it to simulate the temporal and spatial evolution of plasmas generated by 0.53- and 1.06-μm picosecond laser pulses. Contrary to many previous models,[8] emphasis is placed on determining the temperature (T_e) and density (N) of the plasma as well as the temperature (T) of the lattice, all of which are necessary to describe plasma evolution on a picosecond time scale. In Sec. II we provide the coupled transport and balance equations which determine N, T_e, and T, and in Sec. III we offer numerical solutions to these equations for 0.53- and 1.06-μm picosecond laser pulse excitation. The relevant equations are generalized from those presented in our earlier work[7] on nanosecond pulse interactions, which assumed nondegenerate plasmas and $T_e = T$. Because of the many processes which govern plasma evolution, rather than attempt a meaningless multiparameter fit of the model to experimental results, we employ model parameters derived from near-equilibrium experiments from the outset and compare the predictions with experimental results. This is done in Sec. IV where we consider experimental data on the infrared reflectivity and melt threshold of silicon. In performing a realistic assessment of the model we account for effects related to the interaction of pulses of nonzero width and nonzero probe penetration depth with a plasma with strong spatial and temporal inhomogeneties. When this is done we find that the model is able to account for the experimental results and that plasmon assisted recombination and ultrashort carrier momentum relaxation times do not significantly influence plasma kinetics as speculated on in the recent literature. Finally, Sec. V summarizes the salient features of the work.

II. KINETIC EQUATIONS FOR THE COUPLED CARRIER-LATTICE SYSTEM

The fundamental processes which occur during the creation and evolution of laser-generated carriers by short laser pulses have been discussed by many authors including this one.[2] Here we will summarize only those features

of importance to the time scale of the present work (see Fig. 1). The picosecond pulses considered here have energy quanta $\hbar\omega_0$, higher than the band gap E_g of silicon, and absorption of these pulses can occur via single- or two-photon interband absorption or free-carrier absorption. Interband absorption results in the creation of electron-hole pairs with an initial kinetic energy of $(\hbar\omega_0 - E_g)$ while free-carrier absorption events provide individual free carriers with an additional kinetic energy $\hbar\omega_0$. At sufficiently high densities such that carrier-carrier collisions occur on a $< 10^{-13}$ sec time scale the carriers will thermalize into Fermi-Dirac distribution functions on a similar time scale (apart from minor perturbations at optically pumped states during the pulse). The distribution functions for electrons and holes possess different quasi-Fermi levels but a common temperature T_e, which can be higher or lower than the lattice temperature depending on $\hbar\omega_0$. By emission of longitudinal-optic (LO) phonons the carriers attempt to reach thermal equilibrium with the lattice, although they do so initially only with the LO modes. Although the carrier—LO-phonon energy relaxation time τ_E depends in a complicated way on carrier temperature and lattice temperature, we will take it to be constant at[6] 0.5 psec with the view of being conservative in estimating nonequilibrium plasma effects.

Through interactions with the carriers, the population of LO-phonons increases and on a time scale of < 10 psec attempts[9] to thermalize with other lattice modes through phonon-phonon interactions brought about by lattice anharmonicity. Certain phonon states, particularly low-energy, low wave-vector states, may not attain thermal equilibrium populations even after times as long as microseconds. Nevertheless, for times of 10's of picoseconds most of the energy released from the carriers will be deposited in a near-thermal-equilibrium state of the majority of modes and there should be negligible error in assuming internal equilibrium of the lattice at a temperature T on this time scale.

On a suprapicosecond time scale we will therefore assume that the variable T alone can describe the lattice and that the quasiequilibrium temperature T_e and quasi-Fermi levels ψ_c ($c = e,h$ for electrons or holes) can be used to describe the carriers. In the absence of transport effects the microscopic quasi-equilibrium distribution functions for the carriers can then be written as

$$f_c^0(\mathbf{r},\mathbf{p}) = \left[\exp\left[\frac{\pm(E-\psi_c)}{kT_e} \right] + 1 \right]^{-1} , \tag{1}$$

where ψ_c and T_e can depend on position $\mathbf{r}$, while the carrier energy E depends on momentum $\mathbf{p}$ through the dispersion relation of the carriers. The $+$ sign is associated with electrons and the $-$ sign with holes. By integrating over the carrier distribution functions one can obtain the local carrier densities, given by

$$N_c = 2\left[\frac{m_c^* kT_e}{2\pi\hbar^2} \right]^{3/2} \mathcal{F}_{1/2}(\eta_c) , \tag{2}$$

where we have assumed a constant density of states mass m_c^*; η_c is the reduced Fermi level given by

$$\begin{aligned} \eta_e &= \frac{\psi_e - E_C}{kT_e} \quad \text{(for electrons)} , \\ \eta_h &= \frac{E_V - \psi_h}{kT_e} \quad \text{(for holes)} , \end{aligned} \tag{3}$$

with E_C and E_V being the energies of the conduction- and valence-band edges, respectively; the function $\mathcal{F}_j(\cdot)$ is the Fermi-Dirac integral of order j.

Recombination and impact ionization processes allow the electrons and holes to achieve particle number equilibrium at the same temperature T_e. For the carrier densities considered here ($N > 10^{18}$ cm^{-3}) the dominant recombination process is Auger recombination, a three-body interaction in which two carriers recombine, with a third carrier taking up the recombination energy. The effect of Auger recombination is to reduce N, while increasing T_e. The inverse process, impact ionization, occurs when an energetic carrier creates an electron-hole pair, while losing energy itself. From requirements of momentum and energy conservation the initial energy of the impacting carrier must be $> \frac{3}{2}E_g$.

Since optical-absorption rates vary with depth into a sample, N, T_e, and T vary also, giving rise to particle and energy transport. Because the temperatures and densities can vary significantly, typically over distances of less than 1 μm, the large gradients may pose problems for the application of conventional transport theories. Nonetheless, in what follows we will employ an approach based on the classical Boltzmann's equation in the relaxation-time approximation. From a microscopic description we will proceed to a macroscopic description in the form of balance equations for particle number, particle energy, and lattice energy. The key assumptions in this approach are discussed in standard texts.[10] Briefly, we will assume the validity of local quasidistribution functions with quasi-Fermi levels and quasitemperatures, and that these distribution functions do not vary significantly over distances corresponding to the appropriate mean free paths of carriers or phonons. We will also assume that optical pumping rates and recombination rates can be considered to be sufficiently slow so that anisotropic and other state filling

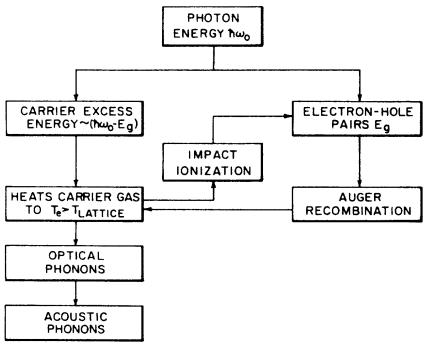

FIG. 1. Schematic diagram of the evolution of laser deposited energy in the carrier and lattice systems; single-photon interband absorption only is considered.

effects[3,11] do not cause significant deviations of the actual distribution functions from the Fermi-Dirac functions. Given the extremes in density, temperature, and gradients of these variables which occur, it is not obvious that all these criteria can be satisfied, although it can be easily checked that they are for the simulations considered here in which the absorption depths are greater than 0.1 μm and the time scale of interest is 10 psec or longer. For shallower absorption depths and/or shorter pulses, or shorter time scales, such may not be the case.

From the relaxation-time approximation of the Boltzmann equation it is easy to show[10] that the electrical and energy currents of the carriers are given by

$$\mathbf{j}_c=\frac{1}{q}\sigma_c\nabla\psi_c-\sigma_c Q_c\nabla T_e \tag{4}$$

and

$$\mathbf{W}_c=(\pi_c-\psi_c)\mathbf{j}_c-\kappa_c\nabla T_e\ , \tag{5}$$

where $-q$ is the charge of an electron, σ_c is the electrical conductivity, Q_c is the Seebeck coefficient, π_c is the Peltier coefficient, and κ_c is the thermal conductivity. These coefficients are given by

$$\begin{aligned}
\sigma_c&=qN_c\mu_c^0\frac{\mathscr{F}_0(\eta_c)}{\mathscr{F}_{1/2}(\eta_c)}\ ,\\
Q_c&=\frac{k}{q}\left[\eta_c-\frac{2\mathscr{F}_1(\eta_c)}{\mathscr{F}_0(\eta_c)}\right]\ ,\\
\pi_c&=T_eQ_c\ ,\\
\kappa_c&=k^2\sigma_c\frac{T_e}{q^2}\left[6\mathscr{F}_2(\eta_c)\mathscr{F}_0(\eta_c)-\frac{4\mathscr{F}_1(\eta_c)^2}{\mathscr{F}_0(\eta_c)^2}\right]\ ,
\end{aligned} \tag{6}$$

where μ_c^0 is the mobility of electrons in a Maxwell-Boltzmann distribution. We have assumed that the energy dependence of the momentum relaxation time is $\propto(E-E_{C,V})^l$ where, for lattice scattering, $l=-\frac{1}{2}$. (Note that the form for the Fermi-Dirac integrals above are explicitly dependent on the particular value of l.)

For a laser-generated plasma, in which both types of carriers move together, the Dember field which develops because of charge separation prohibits the carrier charge and current densities from becoming significantly different so that

$$\mathbf{j}_e=-\mathbf{j}_h,\quad N=N_e=N_h\ . \tag{7}$$

The carrier pair (particle) current is found from

$$\begin{aligned}
\mathbf{J}&=-\frac{1}{q}\mathbf{j}_e=\frac{1}{q}\mathbf{j}_h\\
&=\frac{1}{q^2}\frac{\sigma_e\sigma_h}{\sigma_e+\sigma_h}[\nabla(\psi_h-\psi_e)+q(Q_e+Q_h)\nabla T_e]\ .
\end{aligned} \tag{8}$$

This can be rewritten in terms of N and T_e to give

$$\begin{aligned}
\mathbf{J}&=-D\left[\nabla N+\frac{N}{kT_e}\left[\frac{\mathscr{F}_{1/2}(\eta_e)}{\mathscr{F}_{-1/2}(\eta_e)}+\frac{\mathscr{F}_{1/2}(\eta_h)}{\mathscr{F}_{-1/2}(\eta_h)}\right]\nabla E_g\right.\\
&\quad\left.+\frac{N}{T_e}\left[\frac{2\left[\frac{\mathscr{F}_1(\eta_e)}{\mathscr{F}_0(\eta_e)}+\frac{\mathscr{F}_1(\eta_h)}{\mathscr{F}_0(\eta_h)}\right]}{\frac{\mathscr{F}_{1/2}(\eta_e)}{\mathscr{F}_{-1/2}(\eta_e)}+\frac{\mathscr{F}_{1/2}(\eta_h)}{\mathscr{F}_{-1/2}(\eta_h)}}-\frac{3}{2}\right]\nabla T_e\right]\\
&=-D_0\left[\nabla N+\frac{2N}{kT_e}\nabla E_g+\frac{N}{2T_e}\nabla T_e\right]\quad\text{for }\eta_e,\eta_h\ll-1\ .
\end{aligned} \tag{9}$$

where the band-gap energy is $E_g=E_C-E_V$. The ambipolar diffusivity D is given by

$$\begin{aligned}
D&=\frac{1}{q}\frac{kT_e(\sigma_e\sigma_h)}{\sigma_e+\sigma_h}\left[\frac{\mathscr{F}_{1/2}(\eta_e)}{\mathscr{F}_{-1/2}(\eta_e)}+\frac{\mathscr{F}_{1/2}(\eta_h)}{\mathscr{F}_{-1/2}(\eta_h)}\right]\\
&=D_0\quad\text{for }\eta_e,\eta_h\ll-1\ ,
\end{aligned} \tag{10}$$

where D_0 is the ambipolar diffusivity for a Maxwell-Boltzmann distribution of carriers. Because $\mathscr{F}_j(\eta)/\mathscr{F}_k(\eta)$ increases from unity with increasing η for $j>k$, the diffusion coefficient increases with increasing carrier degeneracy, a result which can be attributed to Fermi pressure. However, the diffusion current does not necessarily reflect this behavior because of the influence of ∇E_g and ∇T_e terms in Eq. (9). In particular, because of the self-energy correction[12] to the particle current, through the ∇E_g term, normal diffusivity can be inhibited and carrier confinement can occur. The self-energy correction results from the dependence of the carrier energy on carrier density through exchange and correlation effects and on lattice temperature, through carrier-lattice interactions. The band-gap gradient can thus be rewritten as

$$\nabla E_g=\frac{\partial E_g}{\partial T}\nabla T+\frac{\partial E_g}{\partial N}\nabla N \tag{11}$$

with the coefficients evaluated from the temperature and density dependence of the band gap as given in Table I.

Ambipolar carrier flow also influences the form of the carrier energy current. From Eqs. (5)–(8) the total ampipolar energy current is

$$\begin{aligned}
\mathbf{W}=\mathbf{W}_e+\mathbf{W}_h&=\left[E_g+2kT_e\left[\frac{\mathscr{F}_1(\eta_e)}{\mathscr{F}_0(\eta_e)}+\frac{\mathscr{F}_1(\eta_h)}{\mathscr{F}_0(\eta_h)}\right]\right]\mathbf{J}\\
&\quad-(\kappa_e+\kappa_h)\nabla T_e\ .
\end{aligned} \tag{12}$$

A. Particle balance

The balance equation for electron-hole pairs becomes

$$\frac{\partial N}{\partial t}+\nabla\cdot\mathbf{J}=G+R\ , \tag{13}$$

where G and R are the pair generation and net recombination rates. The net recombination rate is given by

TABLE I. Model parameters for Si.

Quantity	Symbol	Value
	Thermal and electrical properties	
Lattice thermal conductivity[a]	κ_L	$1585T^{-1.23}$ W/cm K
Lattice specific heat[a]	C_L	$1.978+(3.54\times10^{-4}\ \mathrm{K}^{-1})T-(3.68\ \mathrm{K}^2)T^{-2}$ J/cm^3
Latent heat of melting[a]	$\mathscr{L}$	4000 J/cm^3
Auger recombination coefficient[b]	γ	3.8×10^{-31} cm^6/sec
Impact ionization coefficient[c]	δ	$3.6\times10^{10}\exp(-1.5E_g/kT_e)$ sec^{-1}
Carrier ambipolar diffusivity[c]	D_0	$18(300\ \mathrm{K}/T)$ cm^2/sec
Band gap[d]	E_g	$1.16-7.02\times10^{-4}T^2/(T+1108\ \mathrm{K})-1.5\times10^{-8}N^{1/3}$ eV
	Optical properties	
Reflectivity: (0.53 μm)[e]	Γ	$0.37+5\times10^{-5}(T-300\ \mathrm{K})$
(1.06 μm)[e]		$0.30+5\times10^{-5}(T-300\ \mathrm{K})$
Interband absorption: (0.53 μm)[f]	α	$5.02\times10^3\exp(T/430\ \mathrm{K})$ cm^{-1}
(1.06 μm)[g,h]		(see references)
(1.05 μm)[g,h]		(see references)
Free-carrier absorption: (1.06 μm)[i]	Θ	$5\times10^{-18}(T/300\ \mathrm{K})$ cm^2
(0.53 μm)		(taken as negligible)
Two-photon absorption: (1.06 μm)[j]	β	2 cm/GW
(0.53 μm)		(taken as negligible)

[a]Reference 14.
[b]Reference 15.
[c]Reference 16.
[d]Reference 17.
[e]Reference 18.
[f]Reference 19.
[g]Reference 20.
[h]Reference 21.
[i]Reference 22.
[j]Reference 23.

$R=-\gamma N^3+\delta(T_e)N$, where γ and δ are the Auger recombination and impact ionization coefficients. We will consider for the generation rate

$$G(\mathbf{r})=\frac{(1-\Gamma)\alpha I(\mathbf{r},t)}{\hbar\omega_0}+\frac{(1-\Gamma)^2\beta I^2(\mathbf{r},t)}{2\hbar\omega_0} \tag{14}$$

with $(1-\Gamma)I(\mathbf{r},t)$ the intensity of the optical excitation at $\mathbf{r}$, Γ the reflectivity, α the disorption coefficient for valence–conduction-band transitions, and β the two-photon absorption coefficient. The attenuation of the beam is governed by the one-dimensional equation,

$$\frac{dI}{dx}=-\alpha I-\beta I^2-\Theta N I\ , \tag{15}$$

where x is the depth into the sample and Θ is the free-carrier absorption cross section.

B. Carrier energy balance

The total-energy density in the electron-hole pairs is the kinetic energy plus band-gap energy per unit volume and is given by

$$U=NE_g+\tfrac{3}{2}NkT_e\left[\frac{\mathscr{F}_{3/2}(\eta_e)}{\mathscr{F}_{1/2}(\eta_e)}+\frac{\mathscr{F}_{3/2}(\eta_h)}{\mathscr{F}_{1/2}(\eta_h)}\right], \tag{16}$$

and the total-energy balance equation is

$$\frac{\partial}{\partial t}U+\nabla\cdot\mathbf{W}=S_U-L_U\ , \tag{17}$$

where S_U is the source of total carrier energy heat and L_U is a loss term for total energy in the carrier system. Equation (17) can be converted into a differential equation for T_e by using Eq. (16) together with Eq. (13) for $\partial N/\partial t$.

The only source for total energy in the carrier system is the laser pulse and S_U is given by

$$S_U=(1-\Gamma)I(\mathbf{r},t)(\alpha+\Theta N)I(\mathbf{r},t)+(1-\Gamma)^2\beta I^2(\mathbf{r},t)\ . \tag{18}$$

The loss term is due to loss of kinetic energy through equilibration of the lattice and carrier temperatures and is given phenomenologically by

$$L_U=C_e\frac{T_e-T}{\tau_E}\ , \tag{19}$$

where $C_e=\partial U/\partial T_e\,|_N$ is the electronic specific heat at constant particle number.

Note that impact ionization and Auger recombination do not represent source or loss terms for total carrier energy, since both processes maintain total carrier energy. Nonetheless, Auger recombination, for example, can speed the delivery of carrier energy to the lattice, since carrier ionization energy (E_g) is converted into carrier thermal energy, whose loss rate to the lattice is rapid.

C. Lattice heat balance

With the assumption of internal equilibrium among the phonons the balance of energy in the lattice is given by the usual heat diffusion equation,

$$\frac{\partial T}{\partial t}=C_L\nabla\cdot\kappa_L(\nabla T)-L_U\ , \tag{20}$$

where κ_L is the lattice thermal conductivity and C_L is the lattice specific heat. Because the carrier densities considered here are always much less than 1% of the total electron density, we will assume no self-energy correction to the lattice thermal properties.

Equations (13), (17), and (20) completely determine N, T_e, and T when solved together with the boundary conditions:

$$\left.\frac{\partial N}{\partial x}\right|_{x=0}=0,\quad N(x\to\infty,t)=N_{\rm eq}\simeq 10^{12}\ {\rm cm}^{-3}$$

$$\text{at } T=300\ \text{K},$$

$$\left.\frac{\partial T_e}{\partial x}\right|_{x=0}=0,\quad T_e(x\to\infty,t)=300\ \text{K}, \tag{21}$$

$$\left.\frac{\partial T}{\partial x}\right|_{x=0}=0,\quad T(x\to\infty,t)=300\ \text{K},$$

where surface recombination effects have been neglected on a picosecond time scale. In those simulations involving melting, the solid at the melting point (1685 K) was required to obtain the latent heat energy $\mathscr{L}$ per unit volume before melting occurred.

In the next two sections we will consider explicit computer-generated values of N, T_e, and T for 0.53- and 1.06-μm pulse excitation sources. The values of the parameters used in the simulation are listed in Table I. They are deduced from experiments involving near-equilibrium plasmas or modestly excited Si. It is possible that some of the parameters may be different for highly excited Si due to screening,[13] hot-phonon effects,[9] etc. However, in the absence of definitive, quantitative results about these effects we will neglect them.

III. NUMERICAL SIMULATIONS

A. Interaction of 0.53-μm picosecond pulses with Si

We consider first the interaction of 0.53-μm, 20-psec (full width, half maximum) Gaussian pulses with Si and determine the temporal and spatial evolution or N, T_e, and T for different laser fluences (F). The simulations run from $t=-100$ to 300 psec with the peak of the pulse taken at $t=0$; the sample thickness is taken to be 10 μm, which is large compared to the maximum carrier diffusion depth $\simeq 3$ μm. Since single-photon interband absorption is so strong we can neglect two-photon and free-carrier absorption in the simulations.

Figure 2 shows the time evolution of the surface values of N, T_e, and T for $F=50$- and 150-mJ cm^{-2} pulses. At both values of F the recombination time is always comparable to or greater than the pulse width, and the peak carrier density is reached beyond the peak of the pulse. The peak densities ($<10^{21}$ cm^{-3}) are less than an order of magnitude greater than those achieved with nanosecond excitation.[7] This directly reflects the N^3 dependence of Auger recombination which, along with diffusion, determines the decay characteristics of N. For the carrier temperature, it is interesting to note a two-peak structure in the time dependence of T_e which occurs because both the

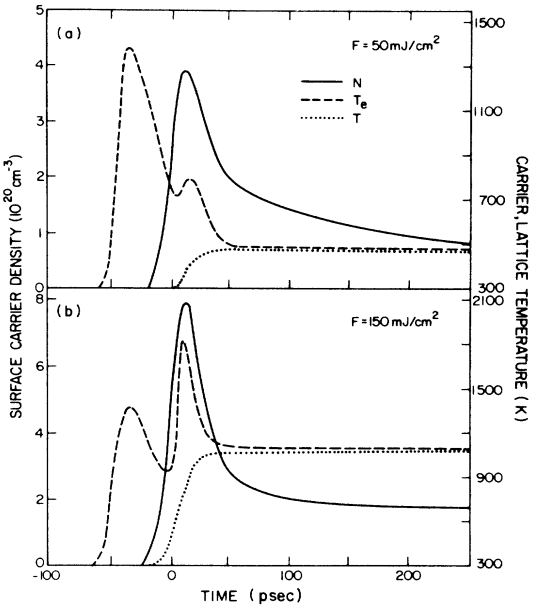

FIG. 2. Carrier density (N), carrier temperature (T_e), and lattice temperature (T) surface values as a function of time for 20-psec, 0.53-μm pulses of fluence: (a) 50 and (b) 150 mJ/cm^2 incident on intrinsic silicon.

laser pulse and rapid Auger recombination heat the plasma and dominate as plasma heat sources at different times during the pulse. At a sufficiently early time on the leading edge of the pulse there is an initial rise in temperature because the pulse is providing energy while not significantly increasing the number of carriers beyond the 10^{12} cm^{-3} already present. The surface carrier temperature peaks at $T_e\simeq 1400$ K at $t\simeq -40$ psec when N has reached a value of $\simeq 10^{14}$ cm^{-3}. T_e then decreases since the pulse is heating an increasingly dense plasma which itself is losing energy to the lattice. Stated differently, the heat capacity of the plasma is increasing faster than the energy content. This is a general effect and not just associated with a Gaussian pulse. However, the temperature at the first peak and its time of occurrence is obviously dependent on the system parameters. T_e again rises near $t\simeq 0$ when the density increases beyond $\simeq 3\times 10^{20}$ cm^{-3}, at which point Auger recombination converts carrier ionization energy into kinetic energy at a sufficiently large rate to again cause the carrier temperature to increase. The peak carrier temperature is, of course, a function of the peak intensity or density. Although T_e begins falling again once the carrier density begins to drop, there remains a significant difference between T_e and T for long times due to on-going Auger recombination. Because T_e is usually much larger than T when N is high, the plasma is never highly degenerate, even at the highest densities where the maximum value of the reduced Fermi levels is at most $\simeq 3$. Nonetheless, one can make an error of as much as a factor of 2 in the transport coefficients, and hence N and T_e, if one assumes Maxwell-Boltzmann statistics. The fact that the carrier temperature can be much higher than

the lattice temperature on a time scale long compared to τ_E or even the pulse width is not surprising because of on-going heating. Indeed, it was demonstrated earlier[24] that, in a steady-state regime for which $N=T_e=0$ (as would be the case near the peak of the pulse), Auger recombination alone leads to a temperature difference given approximately by

$$T_e-T=\frac{(\hbar\omega_0-E_g)\alpha D^{1/2}}{3k[1+\alpha(D\tau_E)^{1/2}]}\frac{\tau_E}{(\tau_R)^{1/2}}\ , \tag{22}$$

where τ_R is the recombination time appropriate for the plasma density. For $N=6\times10^{20}$ cm^{-3} and $\tau_R\simeq8$ psec this gives $T_e-T\simeq1000$ K, in agreement with the more-sophisticated computer results. In nanosecond pulse experiments where $N\lesssim10^{20}$ cm^{-3}, the maximum temperature difference was measured[24] to be $\simeq200$ K, in agreement with Eq. (22). Because of the rapid change in T_e during a picosecond pulse, it would be difficult to verify the value of T_e or its time dependence experimentally using, for example, thermionic emission, unless complete time resolution is obtained.

Impact ionization was determined not to be important in the simulations, although the assumption of a larger value of τ_E (and hence larger T_e) could make it more effective. The impact ionization parameter is perhaps the least well known of all the parameters, and conclusions related to its value must reflect the same uncertainty.

The surface lattice temperature for both fluences rises monotonically with time, and on the time scale of interest here lattice heat diffusion is of no consequence. The rise in temperature occurs not only during the pulse, as hot carriers interact with the lattice, but also after the pulse as recombination energy is given up to the lattice. Because of the presence of high-density carriers on a long time scale, a significant portion of the total deposited laser energy remains in the plasma. This effect is more significant at lower intensities. For example, for 50-mJ cm^{-2} pulses, at the peak of the pulse only 50% of the laser deposited energy is in the lattice while at 100 psec this becomes 80%. For 150-mJ cm^{-2} pulses the corresponding figures are 66% and 95% respectively, reflecting the more rapid Auger recombination during the pulse. At the melting fluence ($\simeq200$ mJ cm^{-2}), 85% of the laser energy is deposited in the lattice within 20 psec after the peak of the pulse, although near the surface the local electronic energy is less than 5% of the local lattice energy, indicating that delayed Auger heating is of little consequence in initiating melting on a 10-psec time scale. Consequences of delayed Auger heating of the lattice are more important for subpicosecond pulse excitation as has recently been observed.[6]

In Fig. 3 we show the spatial profile of N and T, 15 and 200 psec after the pulse maximum of 50- and 150-mJ cm^{-2} pulses. The strong dependence of α on T induces a dramatic change in the spatial profiles of N and T with increasing F. At high F the gradients in T and N increase with time as seen from a comparison of the $t=15$ and 200-psec figures. This effect is aided by the large bandgap gradient which, as stated above, inhibits diffusion and, at high fluences, creates carrier confinement. This causes more energy from Auger recombination to be deposited near the surface, which causes α to increase, steepening the profiles even further. The inhomogeneity of the plasma has a significant influence on its optical properties as discussed below.

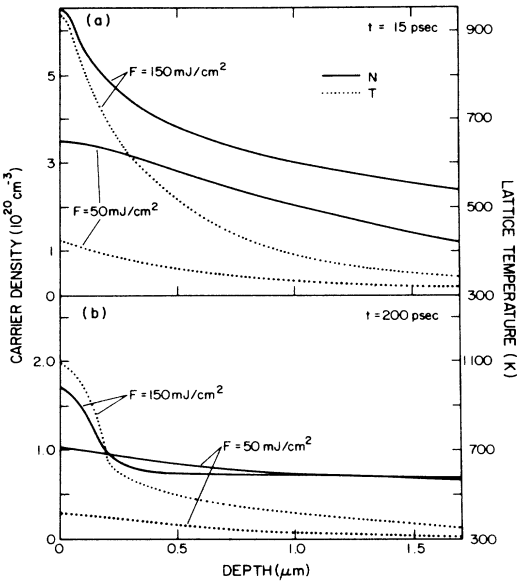

FIG. 3. Spatial profiles of carrier density (N) and lattice temperature (T) following 50 and 150 mJ/cm^2, 20-psec, 0.53-μm pulses incident on silicon for time delays of (a) 15 psec and (b) 200 psec from the peak of the incident pulse.

B. Interaction of 1.06-μm picosecond pulses with Si

In considering the interaction of 1.06-μm pulses with silicon we have taken Gaussian pulses of various widths, partly to simulate recent experiments of Smirl and coworkers.[25] For 1.06-μm radiation α is only 10 cm^{-1} at $T=300$ K, although it increases rapidly with increasing temperature. Higher intensities are therefore required to produce N, T_e, and T values comparable to those of 0.53-μm picosecond pulses. At these higher intensities two-photon processes also become important. Finally, at the longer wavelength, free-carrier absorption cannot be neglected compared to the interband absorption mechanisms. Due to the temperature dependence of α and the increase in free-carrier absorption with NT, T and T_e become highly nonlinear functions of F for pulses of a given width. Indeed, each of these variables is subject to a "runaway" effect as the laser intensity increases. For example, for a 10-psec pulse the peak carrier density achieved for a 0.5-J cm^{-2} pulse is only 7×10^{19} cm^{-3} while for a 1-J cm^{-2} pulse the value is 6×10^{20} cm^{-3}.

In Figs. 4—6 we show results of some of the numerical simulations illustrating the evolution of T, N, and T_e. Figure 4 shows the spatial profiles and increasing gradients which develop in N and T with increasing time during a 8.5-psec pulse at a fluence just below the melting

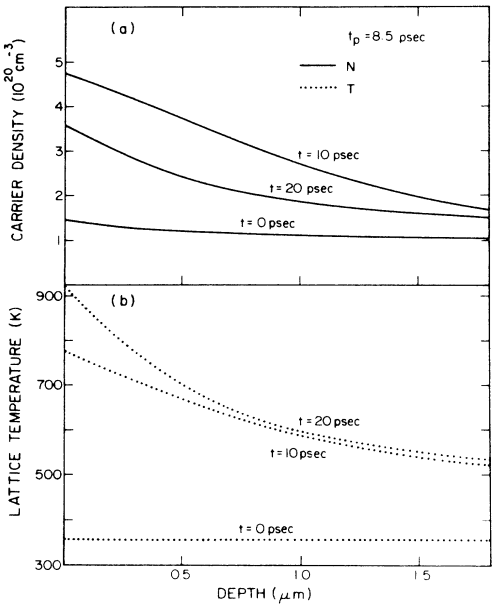

FIG. 4. Spatial profiles at different times for the carrier density (N) and lattice temperature (T) for a 8.5-psec, 1.06-μm excitation pulse at $F=0.95F_{\text{melt}}$.

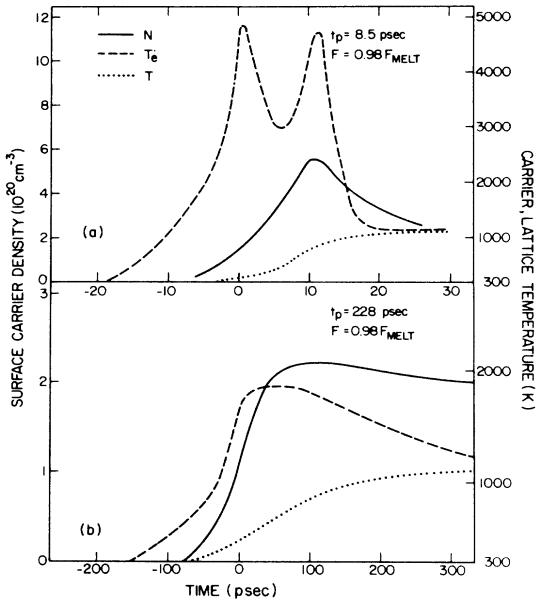

FIG. 6. Carrier density (N), carrier temperature (T_e), and lattice temperature (T) as a function of time during an (a) 8.5-psec, 1.06-μm pulse and (b) 228-psec pulse at $F=0.98F_{\text{melt}}$ in each case. Note change in scales.

threshold fluence. The increasing gradients contribute to the runaway behavior of the surface values of N and T (see Fig. 5). Figure 6 shows the temporal behavior of N, T, and T_e during 8.5- and 228-psec pulses at a fluence just below that of melting. Note that the carrier density achieved can be comparable to that attained with 0.53-μm pulses. For 8.5-psec pulses one observes a two-peak structure in T_e similar to that observed for 0.53-μm excitation. Of note is the rapid increase in T_e to values where there is a possibility of impact ionization, particularly for a reduced band gap at high T. Indeed the inclusion of impact ionization reduces the threshold for melting by about 30% at the shortest pulse widths but has little effect at the longer pulse widths.

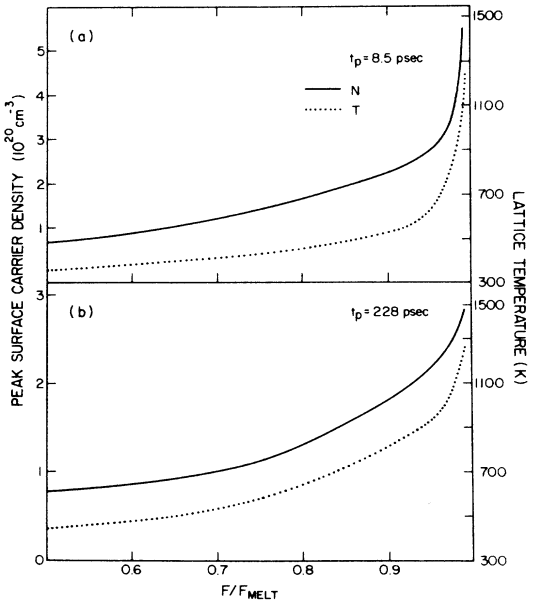

FIG. 5. Lattice temperature (T) and peak carrier density (N) at the surface as a function of laser fluence for 8.5- and 228-psec, 1.06-μm pulses.

Because $(\hbar\omega_0-E_g)$ for $\lambda=1.06$ μm is less than the mean thermal energy of an electron-hole pair at 300 K, carriers which are initially created via single-photon, direct absorption cool to $\simeq$250 K (not indicated in the figure because of the scale) before their temperature increases due to energy deposition by two-photon absorption, free-carrier absorption, etc. later in the pulse.

IV. COMPARISON OF MODEL WITH EXPERIMENTAL RESULTS

Although comprehensive experimental work is not available to test all the effects presented here, especially those related to T_e, we will compare the theory with optical experiments which probe the spatial and temporal characteristics of N. In addition, we will compare predictions of the model with experimental data for the melting threshold.

A. Melting fluence

From the model we find that the threshold fluence for melting by 0.53-μm pulses is 0.19 J cm^{-2} and does not vary significantly with picosecond pulse width, in agreement with experimental data.[1,4] Of course, at this high

fluence, given the high rate of carrier recombination that occurs, together with the short carrier-lattice energy transfer time, the fluence for melting is not particularly sensitive to the carrier dynamics.

The melting fluence for 1.06-μm pulses shows a strong pulse-width dependence since the carrier dynamics strongly influence energy deposition in the lattice. Indeed, as Smirl and co-workers have recently determined,[25] the fluence required for melting ranges from 0.6 to 3 J cm^{-2} for pulse widths between 6 and 228 psec as indicated in Fig. 7. Besides being very sensitive to the pulse width, the fluence does not scale as the room-temperature absorption coefficient for 0.53 and 1.06 μm. Figure 7 shows results of the numerical simulations with and without carrier diffusion and two-photon absorption. It is clear that two-photon absorption and free-carrier absorption are very important[26] processes for 1.06-μm pulses. Although it was suggested earlier[25] that diffusion might explain the dependence of fluence on pulse width, it can be seen from the figure that diffusion plays a negligible role. The main sources[26] for the pulse-width dependence are two-photon absorption and free-carrier absorption, both of which are nonlinear functions of pulse intensity. When free-carrier absorption alone was neglected it was found that the fluence required for melting exceeded 10 J cm^{-2} at all pulse widths.

Diffusion is not important because of the large absorption depths associated with the different absorption mechanisms. Two-photon and direct absorption never produce absorption depths less than a few microns, while free-carrier absorption which is directly proportional to NT only gives an absorption depth of less than 1 μm near the end of the pulses when $N \gg 10^{20}$ cm^{-3} and $T \simeq 1500$ K. By this time there is little time for diffusion to act on the gradients in N that are established. The simulations give good agreement with the experimental results except for the shortest pulses. Some of the assumptions related to the formalism presented in Sec. II are most likely invalid for these short, intense pulses.

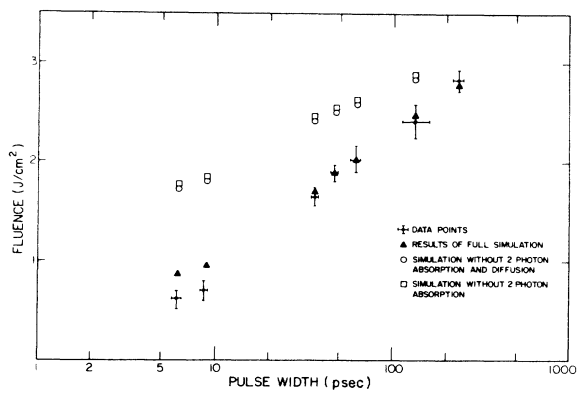

FIG. 7. Fluence threshold for melting as a function of laser pulse width at 1.06 μm. Data taken from Boyd *et al.* (Ref. 25). Note that the two data points with pulse widths less than 10 psec were obtained with 1.05-μm pulses. Results of simulations taking into account various mechanisms are also indicated.

B. Infrared reflectivity

We now wish to consider some recent experiments on the 2.8-μm reflectivity characteristics of plasmas produced in silicon by 0.53-μm pulses. In the last few years, beginning with the work reported by van Driel *et al.*,[5,7,27] first with nanosecond pulses and later with picosecond pulses, there has been interest in the use of infrared reflectivity and transmission techniques for probing plasmas in Si and Ge. There is considerable information in such data which can be assessed once a model for the spatially dependent dielectric constant is obtained. For optical probes where the photon energy $\hbar\omega$ is much smaller than E_g, one can employ a Drude model for the optical properties of the plasma. One must, however, modify this free-carrier description of the dielectric constant[7] in silicon because of strong heavy-hole—to—light-hole and inter-conduction-band transitions,[28] which have been shown to be important in n- and p-doped silicon at high densities. The real and imaginary parts of the dielectric constant can then we written as

$$\epsilon_1 = \epsilon_0 - 4\pi N e^2 \left[\frac{1}{m_e} \left\langle \frac{\tau_e^2}{(1+\omega^2\tau_e^2)} \right\rangle + \frac{1}{m_h} \langle \tau_h^2/(1+\omega^2\tau_h^2) \rangle \right] + 4\pi\chi_i \ ,$$

$$\epsilon_2 = \frac{4\pi N e^2}{\omega} \left[\frac{1}{m_e} \langle 1+\omega^2\tau_e^2 \rangle + \frac{1}{m_h} \langle 1+\omega^2\tau_h^2 \rangle \right] + \frac{4\pi\sigma_i}{\omega} \ ,$$

where $m_{e,h}$ label the electron and hole conductivity effective masses (which, at low densities are $0.26m_0$ and $0.37m_0$, respectively). The $\langle\ \rangle$ brackets indicate averages over the distribution functions of the carriers; χ_i and σ_i are the susceptibility and conductivity associated with interband transitions.

Because of the spatial variation in the dielectric constant due to the inhomogeneity of the plasma, it is important to account for the nonzero skin depth of the probe in reflectivity of transmissivity experiments.[7,29] The effective penetration depth of the probe pulse is given by $c/2\omega n$, where n is the refractive index of the plasma near the surface; for 2.8-μm radiation this depth is >0.1 μm, with the exact value obviously depending on the carrier density. Skin depth corrections therefore become most important when large density gradients or low values of the dielectric constant are present. The reflectivity of an optically inhomogeneous material can be found by using the method of thin films and characteristic matrices as outlined in Ref. 7 or 29. In general, as is easy to show, skin depth effects tend to make the reflectivity (R) closer to its bulk value of 0.30, i.e., lower it if $R > 0.30$ and raise it if $R < 0.30$.

Figure 8 shows typical reflectivity data[5] for Si, excited with a 0.53-μm, 40-mJ cm^{-2} 20-psec pulse and probed at various times with a 2.8-μm pulse of comparable width. The dashed line shows the results of a numerical simulation based on a infinitesmally short probe pulse and assuming an inhomogeneous plasma with a density equal to the surface density. Convolution of the actual probe pulse with this trace, taking into account skin depth, results in

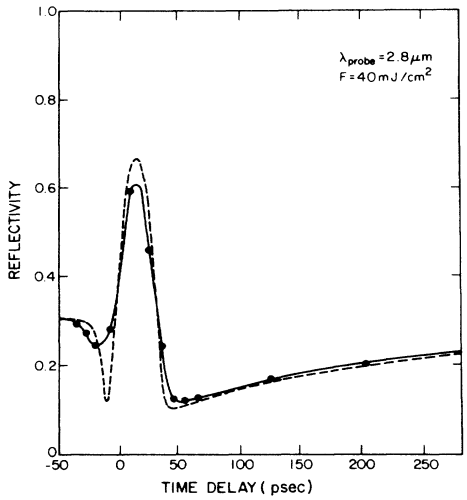

FIG. 8. Silicon reflectivity at 2.8 μm as a function of time during illumination by a 20-psec, 0.53-μm pulse of fluence 40 mJ/cm^2. The dots indicate data taken from van Driel *et al.* (Ref. 5). The dashed line indicates reflectivity, without taking into account the nonzero temporal profile of the pulse and noninfinite spatial profile of the carrier density. The solid line indicates reflectivity taking into account these effects.

an averaging of the instantaneous reflectivity. The results obtained are in good agreement with the data. The initial reflectivity minimum and the maximum are strongly influenced by temporal convolution effects. The second experimental minimum does not differ greatly from its true value; at much lower incident pump fluences the minimum is temporally much broader[9] and the true minimum value of 0.11 is obtained. This value is consistent with damping through interconduction-band transitions[28] and free-carrier damping with $\tau_e = \tau_h \simeq 10^{-13}$ sec.[27] The minimum is theoretically found to occur at a carrier density of 2.1×10^{20} cm^{-3}, slightly less than the value of 2.4×10^{20} cm^{-3} which would be obtained in the absence of damping of the plasmon resonance. The density is less than that for which the effective mass can be expected to increase due to band-nonparabolicity effects.[30] Larger carrier masses likely occur during the pulse, but it would be difficult to extract these masses without very detailed reflectivity data. Note that the position of the second experimental minimum is retarded relative to the position of the true (instantaneous) minimum because of convolution effects. Therefore one must be careful in using the location of the minimum in inferring information about plasma decay characteristics.[12] After the second reflectivity minimum, the difference between the dashed and dotted curves is mainly due to the influence of skin depth effects.

More recent experiments performed using higher pump intensities offer evidence of increasing gradients in the lattice temperature and carrier density and a reduction in diffusion that occurs at high intensities. Evidence for carrier confinement and a reduction in the diffusion coefficient was presented earlier for nanosecond laser induced plasmas in Si as probed by 10.6- and 5.3-μm infrared radiation.[27] Here we show that more dramatic carrier confinement exists for picosecond pulse excitation.

When the pump fluence is increased[31,32] the reflectivity minimum that occurs after the peak of the pulse rises as indicated by the curve in Fig. 9. Kurz and Bloembergen[31] interpreted the increase in the value of the reflectivity minimum as due to strong momentum damping of the plasma by anomalously low momentum relaxation times ($< 10^{-14}$ sec) due to carrier-carrier scattering. This is not likely since the carrier-carrier scattering rate decreases[20] with temperature, in which case the reflectivity minimum should fall. In earlier work[7,27] involving plasmas with densities an order of magnitude less than those considered here, we showed that the plasma momentum relaxation time was dictated by carrier-phonon interactions and had a value of $\simeq 10^{13}$ cm^{-3}. It was also noted that plasma inhomogeneity influences the reflectivity characteristics. From Fig. 3 it is seen that the carrier density gradient increases as a function of fluence due to increasing bandgap reduction, and carrier confinement occurs with increasing lattice temperature. The steepening of the plasma density profile increases the inhomogeneous broadening of the plasmon resonance, leading to an increase in the reflectivity minimum. The dots in Fig. 9 indicate results of a simulation incorporating plasma inhomogeneity effects. Inclusion of the actual temperature dependence of τ_e and τ_h ($\propto T^{-1}$ due to carrier-lattice interactions) yields only a minor contribution to the increase of the reflectivity minimum.

Further evidence of plasma confinement is indicated by the reflectivity[32,33] as a function of fluence at $t = 15$ psec. As seen in Fig. 9, the reflectivity begins decreasing with increasing fluence after approximately 100 mJ cm^{-2}. Rasolt and Kurz[33] explained the reduction of the reflectivity in terms of plasmon assisted recombination, which

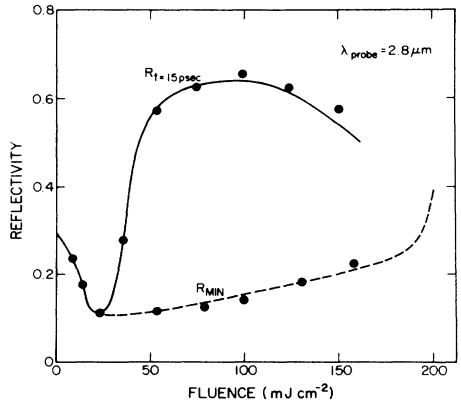

FIG. 9. Reflectivity at 2.8 μm of silicon as a function of fluence for a 20-psec, 0.53-μm excitation pulse. The upper curve indicates data taken from Rasolt and Kurz (Ref. 33) for the reflectivity at 15 psec after the peak of the pulse. The lower curve indicates data taken from Kurz and Bloembergen (Ref. 31) on the minimum reflectivity following the pulse. The dots indicate results of theoretical calculations as outlined in the text.

may become important at very high T and N. Although such recombination may occur, it is not necessary to explain the data. Once again, the reduction of the reflectivity can be explained by the steepening of the carrier density profile due to a reduction of the diffusion coefficient. The dots in Fig. 9 indicate numerical simulations of the reflectivity based on carrier density profiles similar to those of Fig. 3. Good agreement is obtained.

Plasma inhomogeneity effects can also explain transmissivity data in silicon as well as reflectivity and transmissivity data[32] from Ge. Indeed, the effects should be, and are, stronger in Ge since α is always much larger than it is in Si and gradients in N and T are larger.

V. CONCLUSIONS

We have offered a self-consistent formalism for evaluating the kinetics of high-density, high-temperature plasmas generated by 0.53- and 1.06-μm picosecond pulses. Under 0.53-μm excitation the plasma during the pulse is far from thermal equilibrium with the lattice and displays strong spatial inhomogeneity effects which must be accounted for before infrared optical experiments can be correctly interpreted. For 1.06-μm pulses, in spite of the initially low value of α, high carrier densities and carrier temperatures are possible and indeed are instrumental in accounting for the low melting threshold. Two-photon and free-carrier absorption play dominant roles in the energy deposition process leading to melting. Because of the high-temperature and -density gradients that form, none of the four transport terms indicated in Eqs. (4) and (5) can be neglected in determining the energy and particle flow during picosecond optical pulses. Well after these pulses, however, when the gradients have been reduced, Seebeck effects can be neglected in particle flow. The evolution of the near-common T and T_e after the pulse is dictated primarily by lattice thermal conductivity at the lower densities. Finally, it is possible that impact ionization occurs during high-intensity 1.06-μm interaction with Si for which the maximum carrier temperature achieved before melting can be several thousands of degrees, and certainly much higher than that achieved by 0.53-μm excitation. Overall, there is considerable agreement between theory and experiment using model parameters extracted from experiments involving plasmas which are much closer to equilibrium. The only significant discrepancies occur in the determination of the melt threshold of very short 1.06-μm pulses, where high carrier densities and temperatures, and nonequilibrium effects not considered in detail here, may change some of the parameters.

ACKNOWLEDGMENTS

Support for this work from the Natural Sciences and Engineering Research Council of Canada is gratefully appreciated.

[1]See, for example, recent proceedings of the Materials Research Society such as *Energy Beam-Solid Interactions and Transient Thermal Processing,* edited by D. K. Biegelsen, G. A. Rozgonyi, and C. V. Shank (Materials Research Society, Pittsburgh, Pa., 1985).

[2]H. M. van Driel, in *Semiconductors Probed by Ultrafast Laser Spectroscopy,* edited by R. R. Alfano (Academic, Orlando, Fla., 1984), Vol. II, p. 57.

[3]A. L. Smirl, T. F. Boggess, B. S. Wherret, G. P. Perryman, and A. Miller, IEEE J. Quantum Electron. **QE-19**, 609 (1983).

[4]L. A. Lompre', J. M. Liu, H. Kurz, and N. Bloembergen, Appl. Phys. Lett. **44**, 3 (1984).

[5]H. M. van Driel, L.-A. Lompre', and N. Bloembergen, Appl. Phys. Lett. **44**, 285 (1984).

[6]C. V. Shank, R. Yen, and C. Hirlimann, Phys. Rev. Lett. **50**, 454 (1983); M. C. Downer and C. V. Shank, *ibid.* **56**, 761 (1986).

[7]M. I. Gallant and H. M. van Driel, Phys. Rev. B **26**, 2133 (1982).

[8]J. R. Meyer, F. J. Bartoli, and M. R. Kruer, Phys. Rev. B **21**, 1559 (1980); J. R. Meyer, M. R. Kruer, and F. J. Bartoli, J. Appl. Phys. **51**, 5513 (1980); M. Combescot, Phys. Lett. **85A**, 308 (1981); A. Lietola and J. F. Gibbons, J. Appl. Phys. **53**, 3207 (1982).

[9]H. M. van Driel, Phys. Rev. B **19**, 5928 (1979); R. Vasconcellos and R. Luzzi, *ibid.* **22**, 6355 (1980); P. Kocevar, W. Potz, and W. Porod, Physica **117&118B**, 220 (1983); E. J. Yoffa, Phys. Rev. B **21**, 2415 (1980); E. J. Yoffa, *ibid.* **23**, 1909 (1981).

[10]H. J. Kreuzer, *Nonequilibrium Thermodynamics and its Statistical Foundations* (Clarendon, Oxford, 1981); J. R. Drabble and H. J. Goldsmid, *Thermal Conduction in Semiconductors* (Pergamon, New York, 1961), p. 203.

[11]J. L. Oudar, D. Hulin, A. Migus, A. Antonetti, and F. Alexandre, Phys. Rev. Lett. **55**, 2074 (1985).

[12]H. M. van Driel, J. S. Preston, and H. M. van Driel, Appl. Phys. Lett. **40**, 385 (1982); J. F. Young and H. M. van Driel, Phys. Rev. B **26**, 2147 (1982); J. A. Van Vechten and M. Wautelet, *ibid.* **23**, 5551 (1981).

[13]E. J. Yoffa, Phys. Rev. B **21**, 2415 (1980); **23**, 1909 (1981).

[14]R. F. Wood and G. E. Giles, Phys. Rev. B **23**, 2923 (1981).

[15]J. Dwiezor and W. Schmid, Appl. Phys. Lett. **31**, 346 (1977).

[16]S. M. Sze, *Physics of Semiconductor Devices* (Wiley, New York, 1969), p. 60; J. Geist and W. K. Gladden, Phys. Rev. B **27**, 4833 (1983).

[17]Y. P. Varshni, Physica **34**, 149 (1967).

[18]G. E. Jellison and F. A. Modine, Phys. Rev. B **27**, 7466 (1983).

[19]G. E. Jellison and F. A. Modine, Appl. Phys. Lett. **41**, 180 (1982).

[20]G. E. Jellison and D. H. Lowndes, Appl. Phys. Lett. **41**, 594 (1982).

[21]G. G. MacFarlane, T. P. McLean, J. E. Quarrington, and V. Roberts, Phys. Rev. **111**, 1245 (1958).

[22]K. G. Svantesson, J. Phys. D **12**, 425 (1979).

[23]T. F. Boggess, Jr., K. M. Bonhert, K. Mansour, S. C. Moss, I. W. Boyd, and A. L. Smirl, IEEE J. Quantum Electron.

QE-22, 360 (1986).
[24]T. L. F. Leung and H. M. van Driel, Appl. Phys. Lett. **45**, 683 (1985).
[25]I. W. Boyd, S. C. Moss, T. F. Boggess, and A. L. Smirl, Appl. Phys. Lett. **45**, 80 (1984).
[26]H. M. van Driel and A. L. Smirl, Appl. Phys. Lett. (to be published).
[27]J. S. Preston and H. M. van Driel, Phys. Rev. B **30**, 1950 (1984).
[28]M. Balkanski, A. Aziza, and E. Amzallag, Phys. Status Solidi **31**, 323 (1969); L. M. Lambert, *ibid.* **11a**, 461 (1972).
[29]I. F. Vahknenko and V. L. Strizhevskii, Fiz. Tekh Poluprovodn. **3**, 1844 (1969) [Sov. Phys.—Semicond. **3**, 1562 (1970)].
[30]H. M. van Driel, Appl. Phys. Lett. **44**, 617 (1984).
[31]H. Kurz and N. Bloembergen, in *Energy Beam-Solid Interactions and Transient Thermal Processing,* edited by D. K. Biegelsen, G. A. Rozgonyi, and C. V. Shank (Materials Research Society, Pittsburgh, Pa., 1985), Vol. 35, p. 3.
[32]A. M. Malvezzi, C. Y. Huang, H. Kurz, and N. Bloembergen, in *Beam Solid Interactions and Phase Transformations in Solids,* Proceedings of the Materials Research Society, edited by H. Kurz, G. L. Olson, and J. M. Poate (Materials Research Society, Pittsburgh, Pa., 1986), Vol. 31, p. 201.
[33]M. Rasolt and H. Kurz, Phys. Rev. Lett. **54**, 722 (1985).